ELSEVIER Nuclear Instruments and Methods in Physics Research A 403 (1998) 442–454

NUCLEAR INSTRUMENTS & METHODS IN PHYSICS RESEARCH Section A

Use of ^{4}He-filled proportional counters as neutron spectrometers

M. Weyrauch[a,*], A. Casnati[a,b], P. Schillebeeckx[b], M. Clapham[c]

[a] *Physikalisch-Technische Bundesanstalt, D-38116 Braunschweig, Federal Republic of Germany*
[b] *EC, JRC Ispra, Institute for Systems, Informatics and Safety, I-21020 Ispra, Italy*
[c] *BNFL Instruments Ltd., Pelham House, Calderbridge, Cumbria CA20 1DB, UK*

Received 18 September 1997

Abstract

Neutron response functions of two commercially available cylindrical ^{4}He-filled proportional counters (filling pressure about 2 MPa) have been measured in the neutron energy range 144–14 000 keV. Measurements were carried out using optimal settings for the detector high voltage and amplifier shaping time which were determined within the scope of this study. The experimental results have been analyzed and compared to calculated response functions using empirically determined energy and resolution calibration functions.

The theoretically determined response functions show good agreement with the measured response except for energies above 10 MeV. The discrepancies are attributed to unsatisfactory electronics. The Monte-Carlo code Gas-filled neutron spectrometer response (GNSR) which has been developed for the calculation of response functions and efficiencies of gas-filled neutron detectors, is briefly described. © 1998 Elsevier Science B.V. All rights reserved.

PACS: 20.30.Hs; 29.40.Cs

1. Introduction

Gas-filled proportional counters are widely used in the field of neutron spectrometry. Proton recoil proportional counters, in particular, are often used and are well understood. Since the neutron–proton elastic cross section is very well known, this type of counter is particularly useful for high-precision neutron spectrometry. Examples of the successful application of gas-filled neutron spectrometers are given in Refs. [1–5]. The H_2-filled proportional counters are generally operated at low filling pressures (a few hundred kPa). These detectors show almost direct proportionality between measured pulse height and kinetic energy of the charged particles involved in the nuclear reaction. For such detectors the total response, including the wall effect, can be obtained using Monte-Carlo calculations or from analytical expressions [1,6–8].

Because of the low filling pressure, the application of these detectors in neutron spectrometry is restricted to neutron energies below about 2 MeV. The low stopping power of charged particles within these detectors means that higher-energy events cannot deposit their full kinetic energy inside the counter due to wall effects. Another restriction is

* Corresponding author. Tel.: + 49 531 592 7511; fax: + 49 531 592 8106; e-mail: michael.weyrauch@ptb.de.

0168-9002/98/$19.00 © 1998 Elsevier Science B.V. All rights reserved
PII S0168-9002(97)01132-7

the low detection efficiency due to small nuclear reaction cross sections. It has therefore been proposed to use ^{4}He at high pressure (1–2 MPa) as a filling gas [9].

The investigation and successful application of ^{4}He-filled neutron spectrometers started in about 1970 [10–12]. Ref. [12] presents a detailed summary of neutron spectrometry using ^{4}He-filled proportional counters. Problems attributed to the nonlinear relationship between the charged particle kinetic energy released inside the detector and the charge collected at the anode wire are discussed. This problem was also reported by Shamu [13] for gas scintillation neutron spectrometers with high ^{4}He filling pressure. It is also suggested that the detector response could be influenced by neutron-induced charged particle reactions in the counter wall. To reduce this influence, Birch [12] proposed a lead-lined counter. These two problems are investigated in this paper during the characterization of two commercially available ^{4}He proportional counters for use as neutron spectrometers.

For neutron spectrometry applications above 1 MeV neutron energy, detectors filled with ^{4}He seem to be particularly suitable due to the behaviour of the ^{4}He elastic neutron scattering cross section as a function of neutron energy. This cross section is shown in Fig. 1 in comparison to both the ^{3}He(n, p) cross section and the elastic neutron–proton scattering cross section.

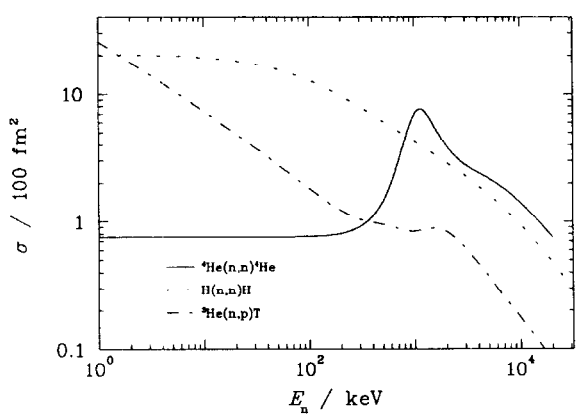

Fig. 1. The neutron elastic scattering cross section for hydrogen and ^{4}He, and the (n, p) cross section of ^{3}He as given in ENDF/B6 [14].

The recorded pulse height spectrum obtained from a ^{4}He-filled proportional counter represents a convolution of the incident neutron energy spectrum with the detector response. Therefore, it is clear that deconvolution of the detector response from the pulse height spectrum will yield the neutron energy spectrum. Such a deconvolution is only possible if a detailed and accurate description of the detector response is available. Section 2 outlines the calculation of the response functions using the Gas-filled Neutron Spectrometer Response (GNSR) code which has been devised to calculate response functions of various gas-filled proportional counters [15,16]. Furthermore, an outline of the procedure used to determine the energy and resolution calibration for a detectors [17] is given. In Section 3, optimization of the settings for the detector high voltage and the amplifier shaping time is described. A comparison of measured and calculated response functions in the neutron energy range from 144 keV to 14 MeV is presented in Section 4.

2. Response functions

Response functions of neutron detectors can be either measured in high-precision reference fields or calculated by simulation techniques. Unfolding recorded pulse height spectra requires a detailed representation of the detector response over the entire range of neutron energies that will be measured. Such a representation is obtained in matrix form with each column containing the detector response to a monoenergetic neutron beam of progressively higher energy. The response matrix can hardly be obtained experimentally, which means that a method of calculation is essential. The method used to calculate detector response functions must be validated by comparing calculated response functions with measured detector responses in quasi-monoenergetic neutron fields. The procedure used to obtain a calculable response is described in the following.

2.1. Structure of the response functions

Consider an extended neutron source with a source number density $S(\boldsymbol{p}_n, \boldsymbol{x}_n)$ of neutrons emitted

with momentum $\boldsymbol{p}_n$ and energy E_n at position $\boldsymbol{x}_n$ per unit time. The source density is normalized such that

$$\int \mathrm{d}^3 p_n \int \mathrm{d}^3 x_n \, S(\boldsymbol{p}_n, \boldsymbol{x}_n) = \dot{N}, \tag{1}$$

$\dot{N}$ being the total rate of neutrons produced. The x_n integration extends over the source volume.

A neutron which traverses the detector volume may deposit some or all of its kinetic energy via nuclear interactions and subsequent atomic processes inside the detector volume. However, it is possible that not all of the incident neutron's kinetic energy will be detected. For example, if charged particles born as a result of neutron interactions within the detector hit the detector wall prior to depositing all of their energy this energy is lost from detection. It is also likely that some of the neutron energy may be carried out of the detector by scattered neutral particles, for example, elastically scattered neutrons in the case of a ^{4}He-filled detector. The process of energy deposition inside the detector is complicated and can be calculated only in suitable approximations. The analytically or numerically determined approximation of the deposited energy E_c is a function of many variables, one of which is the incoming neutron energy $E_n = p_n^2/2m_n$ with the neutron mass denoted by m_n. For simplicity, in the following we will write $E_c = E_D(E_n)$, where E_D denotes the functional dependence of the deposited energy E_c on the various variables.

The distribution $C(E_c)$ of energy E_c is then calculated as follows:

$$C(E_c) = \int \mathrm{d}^3 p_n \int \mathrm{d}^3 x_n \, S(\boldsymbol{p}_n, \boldsymbol{x}_n) I(\boldsymbol{p}_n, \boldsymbol{x}_n) \times \delta(E_c - E_D(E_n)). \tag{2}$$

This expression is written in terms of the quantity $I(\boldsymbol{p}_n, \boldsymbol{x}_n)\delta(E_c - E_D(E_n))$ representing the probability density of an incoming neutron, created at point $\boldsymbol{x}_n$ with momentum $\boldsymbol{p}_n$, to deposit energy E_c. This quantity depends on various interaction cross sections as will be discussed below. The normalization of $C(E_c)$ is obviously given by

$$\int \mathrm{d}E_c C(E_c) = \dot{n}, \tag{3}$$

with $\dot{n}$ being the rate of neutrons interacting inside the detector. Note that this rate is usually much lower than the rate of neutrons traversing the detector volume, since most neutrons will not interact with the detector gas.

For many practical applications the source density S is separated into a neutron energy-dependent part $\Phi(E_n)$ and an angular dependence $s(\Omega_{p_n}, \boldsymbol{x}_n)$,

$$S(\boldsymbol{p}_n, \boldsymbol{x}_n) = \Phi(E_n) s(\Omega_{p_n}, \boldsymbol{x}_n) \tag{4}$$

with Ω_{p_n} being the solid angle of the neutron momentum. This separation can be shown to be approximately valid for many practical neutron sources [15], if neutron interactions within the source can be neglected. The normalization is chosen such that

$$\int \mathrm{d}E_n \, \Phi(E_n) = \dot{N}. \tag{5}$$

Then the angular variables in Eq. (2) are integrated out to obtain

$$C(E_c) = \int \mathrm{d}E_n \, R(E_c, E_n) \, \Phi(E_n) \tag{6}$$

with the response function

$$R(E_c, E_n) = \int \mathrm{d}\Omega_{p_n} \int \mathrm{d}^3 x_n \, s(\Omega_{p_n}, \boldsymbol{x}_n) I(\boldsymbol{p}_n, \boldsymbol{x}_n) \times \delta(E_c - E_D(E_n)). \tag{7}$$

A computer code to calculate Eq. (7) will be described in the following subsection.

Unfortunately, Eq. (2) or Eq. (7) are only approximations since, in practice, the function $E_D(E_n)$ and the interaction probability I can hardly be calculated with sufficient accuracy. Electronic effects (e.g. gas multiplication, recombination, statistical effects) which determine the deposition of energy within the detector are too complex to describe in detail. Moreover, details of the detector geometry and construction may not be well known. In order to account for such effects the following procedure is adopted: The calculated distribution $C(E_c)$ is folded with a (possibly nonlinear) relationship ε between calculated energy E_c and the charge

collected at the anode wire E_d, $E_d = \varepsilon(E_c)$.

$$D(E_d) = \int dE_c \delta(E_d - \varepsilon(E_c))C(E_c). \quad (8)$$

The charge collected at the anode wire is used as a measure of the energy deposited in the detector. The relationship $\varepsilon(E_c)$ must be determined by experiment as will be described below. This process will be called "energy calibration" of the detector.

Consideration must also be given to the statistical fluctuations in the detected energy. This effect is included in the calculated response by folding the distribution $D(E_d)$ with a Gaussian. The Gaussian width is energy dependent and must, therefore, also be determined experimentally in a procedure called resolution calibration.

$$P(E) = \int dE_d\, D(E_d)G(E - E_d) \quad (9)$$

with

$$G(E - E_d) = \frac{1}{\sqrt{2\pi}\sigma(E_d)} \exp\left(-\frac{(E - E_d)^2}{2\sigma^2(E_d)}\right). \quad (10)$$

In summary, the response functions may be written in terms of the following expression:

$$P(E) = \int dE_c\, G(E - \varepsilon(E_c))C(E_c)$$

$$= \int dE_c \int dE_n\, G(E - \varepsilon(E_c))R(E_c, E_n)\Phi(E_n) \quad (11)$$

which depends on the calculated response R and two functions to be determined phenomenologically, the energy calibration function ε and the resolution function σ. Experimental data will be analyzed using this formula.

2.2. Calculation of the "ideal" response

The response function R defined in Eq. (7) is called the ideal response function, since it describes a detector with a calculable response. To calculate R, the computer program GNSR has been developed. This program is devised to calculate response functions for proportional counters filled with H_2, ^3He or ^4He and mixtures of these gases with CO_2, CH_4, Kr, and Xe. However, extensions to other gas fillings are easily implemented.

The program is confined to binary nuclear reactions in the detector gas and neglects multiple neutron scattering, so that the interaction probability I can be written as

$$I(\boldsymbol{p}_n, \boldsymbol{x}_n) = \int d^3p_1 \int d^3x_1$$

$$\times \int d\eta \sum_i \rho_i(\boldsymbol{x}_1) \frac{d^3\sigma_i(E_n)}{d^2\Omega_1\, dE_1} \frac{1}{p_1 m_1}$$

$$\times \delta(\boldsymbol{x}_1 - \eta\hat{\boldsymbol{p}}_n - \boldsymbol{x}_n). \quad (12)$$

A cylindrical detector geometry is assumed and the x_1 integration is limited to the detector volume. The δ-function serves to restrict this integration to the traversal line of the neutron within the detector volume, i.e. nuclear reactions can take place only on this line. The variables p_1 and m_1 denote the momentum and the mass of one of the particles created in the binary nuclear reaction. The number density of the different nuclear components i of the gas is denoted by ρ_i. This quantity is calculated by the program from the chemical composition of the gas molecules and their densities. The differential cross sections of the reactions $d^3\sigma_i(E_n)/d^2\Omega_1\, dE_1$ have to be known from independent sources. A small database of relevant cross sections extracted from Ref. [14] is supplied with the program.

The program calculates the detector response from Eq. (7) in various neutron beam configurations: point source, isotropic source, parallel beam, extended cylindrical source, and a plane rectangular localized source. The energy $E_c = E_D(E_n)$ is calculated using range data for the charged particles created in the nuclear reactions and the detector geometry. In the database supplied with the program, a selected set of relevant range data is provided. The applicability of the program is limited to non-relativistic energies. Scattering and reactions in the detector wall or other parts of the detector are not taken into account in the present version of the code. Ref. [15] gives a detailed description of the capabilities of the code and provides a User Manual. The calculated response functions are output in a format suitable for direct input into the

HEPRO unfolding package compiled by Matzke [18].

2.3. Energy and resolution calibration

As was noted before, our final expression, Eq. (11), for the response depends on two functions $\varepsilon(E_c)$ and $\sigma(\varepsilon)$. These functions will be suitably parameterized in the following and determined from experimental data. The relationship between the calculated energy E_c and ε may be written as a power series expansion

$$\varepsilon(E_c) = a_0 + a_1 E_c + a_2 E_c^2 + \cdots . \tag{13}$$

Ideally, the two quantities are strictly proportional. Similarly, one writes a power series expansion for the resolution function

$$\sigma^2(\varepsilon) = b_0 + b_1 \varepsilon + b_2 \varepsilon^2 + \cdots . \tag{14}$$

Both the energy calibration function, Eq. (13), and the resolution calibration function, Eq. (14), describe effects of the detector as well as the electronics of the measurement system not taken care of in the detector simulation.

To determine the functions ε and σ measurements of $P(E)$ are performed in particularly well known and nearly monoenergetic neutron fields $\Phi(E_n)$ with the detector to be calibrated. The detailed form of the calibration field $\Phi(E_n)$ is obtained either from calculations of the neutron production target or from independent measurements. The detector response R is calculated in accordance with the previous subsection so that the only unknowns in Eq. (11) are the parameters of the Gaussian, ε and σ. Unfortunately, in the case of recoil proportional counters, R is a function of E_c supported on the interval from zero up to the maximum recoil energy E_c^{max}. In order to determine ε and σ for a particular E_c from the measured $P(E)$, it is sufficient to fit the measured spectrum near the upper edge of the measured response, i.e. we consider only E_c near the E_c^{max}. From this fit we determine $\varepsilon(E_c^{max})$ and the relative resolution $\sigma(\varepsilon)/\varepsilon$ at $\varepsilon(E_c^{max})$. This procedure is repeated with several nearly monoenergetic neutron beams. From these results the parameters a_i and b_i in Eqs. (13) and (14) can be determined. For an ideal detector one expects in Eq. (13) $a_0 = 0$ and $a_i = 0$ for $i \geq 2$, i.e. linear in energy. This is never exactly so in practical cases. If we define a function $\alpha(E_c)$ as

$$\varepsilon(E_c) = \alpha(E_c) E_c, \tag{15}$$

then α will be constant for a "good" detector as defined above. If α is not constant this indicates a nonlinear energy deposition and/or a nonzero offset a_0 in the detector system. We will analyze our results using this representation in Section 4.

To find the best operating conditions, i.e. as close to the ideal case as possible, the procedure described above is repeated for different operational settings. The operational settings available for optimization were: the high voltage applied between the anode and the cathode of the detector and the shaping time of the amplifier. Once suitable parameter functions ε and σ had been determined, the measured and the calculated pulse height distribution [Eq. (7)] should agree. The validity of such comparisons made during the course of this study will be discussed in detail.

3. Setup of the detector systems

The basic characteristics of the two cylindrical ^{4}He proportional counters under study are summarized in Table 1. Both devices are commercially available from the manufacturers indicated and will be referred to as TGM and RS. The measurement electronics consisted of a charge-sensitive preamplifier and a Gaussian pulse shaping main amplifier. Since the stopping power of electrons above 200 keV is almost a constant (about 6 keV/cm in ^{4}He at a pressure of 1.5 MPa), the maximum energy deposited in the detector due to gamma rays interacting with the detector wall is 300 keV for the RS detector and 600 keV for TGM detector. As a consequence, an n-γ discrimination system was not necessary for the measurements reported in this paper.

The optimum high-voltage setting has been determined by a number of measurements in a variety of neutron fields. For the TGM detector a similar device doped with a trace of ^{3}He was available, which was exposed to a thermal neutron beam from a neutron source placed in polyethylene. The resolution of the 764 keV peak was

Table 1
Characteristics of the ^{4}He proportional counters

Detector	Pressure (MPa)	Composition of gas filling (%)	Anode radius (μm)	Inner radius (cm)	Effective length (cm)	Effective volume (10^{-3} m^3)
TGM (TGM Centronics) Type: 100 HE4/1140/50S 9504-18	1.520	98.5 ^{4}He 1.5 CO_2	25.4	2.451	100.076	1.889
RS (Reuter & Stocks) Type: RS-P5-1620-203	1.551	99.0 ^{4}He 1.0 CO_2	12.5	2.42	49.88	0.918

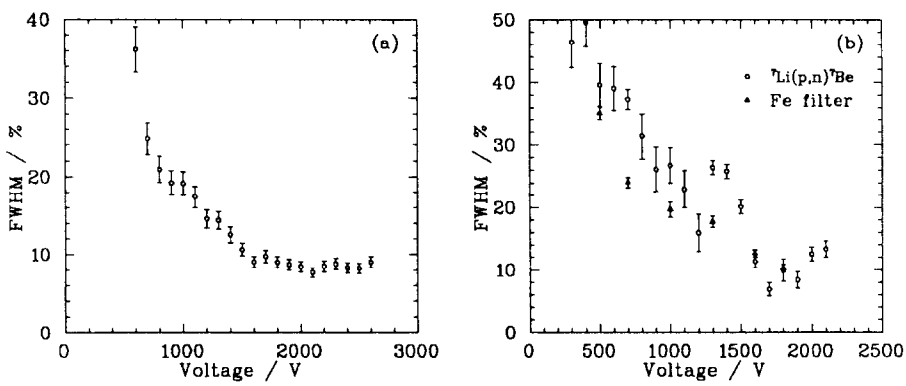

Fig. 2. Relative resolution of the TGM (a) and RS (b) detectors as a function of high voltage measured in the neutron fields described in the text.

studied as a function of both the detector high voltage and amplifier shaping time. The RS detector was exposed to two different neutron beams: the iron-filtered reactor beam of PTB (this provides a well characterized multi-line spectrum extending to a neutron energy of about 1 MeV) and the 2.7 MeV proton accelerator beam at the University of Tübingen using the ^{7}Li(p, n)^{7}Be reaction ($E_n \approx 1$ MeV).

Fig. 2 summarizes measurements of the detector resolution at various high-voltage settings. These data yield the best resolution when the high voltage is set between 2000 and 2300 V for the TGM detector and between 1600 and 1900 V for the RS detector.

Using a high-voltage setting of 1600 V for the RS detector, measurements with varying shaping times have been performed. The influence of the shaping time was studied in two geometries: the neutron beam parallel and perpendicular to the anode wire. The response to an 8 MeV neutron beam in both geometries is shown in Fig. 3. For the parallel measurements (Fig. 3b), a ballistic deficit without significant loss of resolution is observed. Such an effect can be explained by a constant relative ballistic deficit due to the long drift time of the secondary positive ions. The primary ionization tracks of the high-energy alpha particles are parallel to the anode wire, resulting in a constant electron drift time.

The response functions obtained with the neutron beam perpendicular to the anode wire (Fig. 3a) show that the ballistic deficit causes a considerable loss of resolution and linearity for short shaping times. This is due to the spread in electron drift times of the primary electrons along the track. Because the ranges of the alpha particles scattered perpendicular to the anode wire are in the order of the detector radius a spread in electron drift times in the order of 20 μs is expected. As a consequence, large shaping times should be used to avoid losses of energy resolution and linearity.

The improvement achieved using a gated integrator system as described in Ref. [19] is shown in Fig. 4 for responses to a 2.5 MeV and 14.86 neutron beam perpendicular to the anode wire. The full line in Fig. 4 represents the calculated response using energy calibration functions ε and resolution σ as described in Section 4. For 2.5 MeV neutron beam, no significant difference between the responses in shape and resolution is observed. For the 14.86 MeV neutron beam, a considerably better agreement with the theoretically determined response is obtained using the gated integrator.

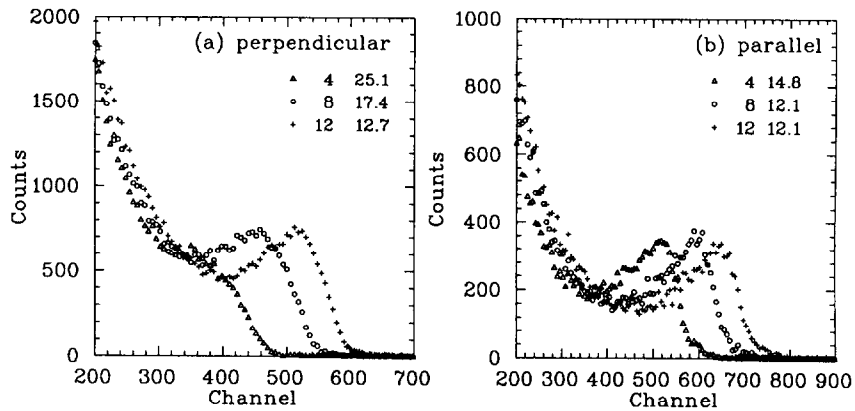

Fig. 3. The response of the RS detector to a 8 MeV neutron beam (a) perpendicular and (b) parallel to the anode wire for different shaping times (in μs) of the Gaussian shaping amplifier. The relative resolution (FWHM / %) is also indicated.

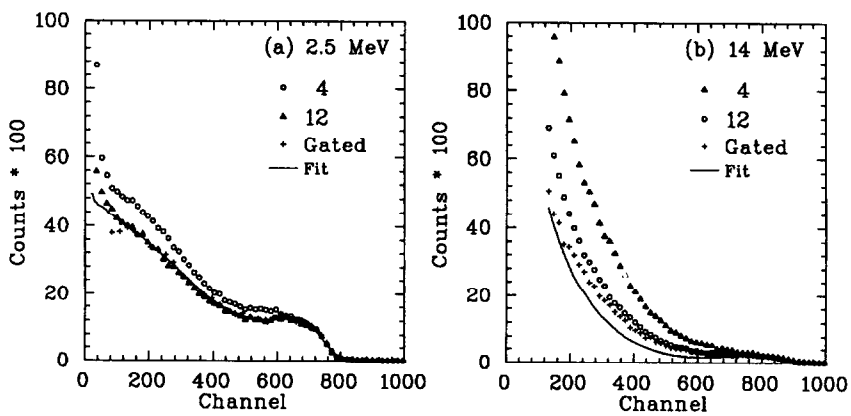

Fig. 4. The RS detector response to a 2.5 MeV (a) and 14.86 MeV (b) neutron beam *perpendicular* to the anode wire. Response functions obtained with a Gaussian shaping amplifier (4 and 12 μs shaping time) and a gated integrator circuit [19] are compared. The response functions were calibrated on a common channel grid using parameter a_1 [Eq. (13)] obtained by a least-squares fit procedure.

Systematic improvements have been observed in the shape and resolution of the spectra obtained with larger shaping times, further improvements are noted when using a gated integrator circuit. This suggests that a system capable of handling pulses with very long rise times is essential.

4. Measured response functions

Measurements with the TGM detector were performed at the Van de Graaff accelerator facility at the Istituto Nazionale di Fisica Nucleare (INFN) in Legnaro, Italy. The detector was exposed to neutron beams with energies between 450 and 4500 keV. These neutron beams were obtained from the Li(p, n) reaction in a 700 μg/cm^2 thick LiF target and a 440 nA proton current. All measurements were performed with the anode wire of the detector perpendicular to the direction of the neutrons emitted at zero degrees and at a distance of 2.48 m from the target. Shadow cone measurements to account for the scattered (background) neutron fluence have not been done. The neutron spectrum $\Phi(E_n)$ incident on the detector was calculated by a Monte-Carlo code that accounts for the energy loss of the protons in the target and the cross-sections of the ^{7}Li(p, n)^{7}Be and the ^{7}Li(p, n)^{7}Be* reactions [20].

From the measurements obtained at the INFN it is possible to calibrate the detector for both energy and resolution. The functions α [see Eq. (15)] and the relative resolution σ (FWHM in %) as a function of the maximum recoil energy ($E_c^{max} = 4E_n m_4 m_n/(m_4 + m_n) = 0.64E_n$) are shown in Fig. 5. These results were obtained using a Gaussian shaping amplifier with 8 μs shaping time and a high-voltage setting of 2300 V.

The nonlinear behavior of the energy calibration is described by two phenomenological expressions [17],

$$\alpha(E_c) = G\left(1 - \frac{E_0}{E_c}\exp\left(\frac{aE_c}{1 + bE_c}\right)\right), \tag{16}$$

and

$$\alpha(E_c) = \frac{G}{E_c}\int_0^{E_c} \frac{dE}{1 + B\,dE/dx}, \tag{17}$$

where G, a, b, E_0 and B are adjustable fit parameters and dE/dx is the stopping power of the charged particles in the detector taken from Ziegler [21]. The full line in Fig. 5a is the result of a least squares fit to the data points using Eq. (16) with the parameters given in Table 2. Using Eq. (17) similar agreement is obtained (dashed line in Fig. 5). Eq. (16) was developed following the suggestion of Finch [22] that the nonlinear behaviour observed in ionization chambers and surface barrier detectors was due to nuclear interactions and recombination of charge carriers. Eq. (17) has been suggested by Birks [23,24] to describe the nonlinearities in

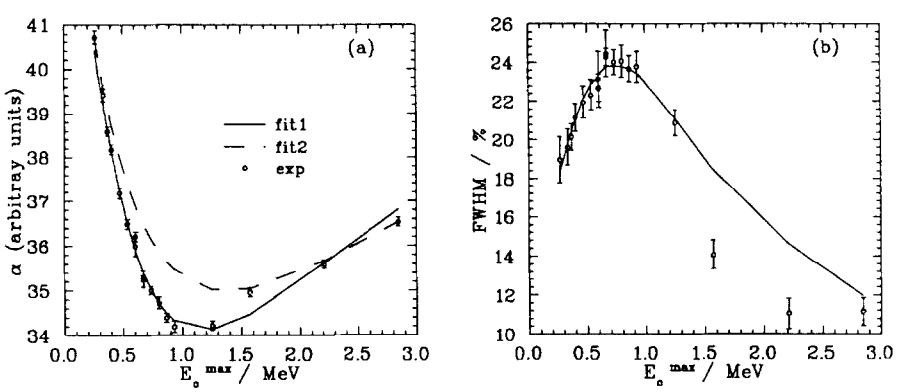

Fig. 5. (a) The function $\alpha(E_c^{max})$ [see Eq. (15)] determined from measurements with the neutron beam *perpendicular* to the anode wire using the TGM detector. The curve labelled "fit1" is obtained from Eq. (16) and the curve labelled "fit2" from Eq. (17) using the parameters given in Table 2. (b) The relative resolution (FWHM). The full line is obtained from Eq. (18) using the parameters given in Table 2.

Table 2
Parameters obtained for the phenomenological description of the energy deposition and the resolution. The parameters without uncertainty have been set as constraints and are not fitted

Detector	TGM	RS perpendicular	RS parallel
a (keV^{-1})	$(28.5 \pm 0.2) \times 10^{-3}$	$(23.1 \pm 0.4) \times 10^{-3}$	$(27.2 \pm 0.6) \times 10^{-3}$
b (keV^{-1})	$(40.7 \pm 0.3) \times 10^{-4}$	$(32.5 \pm 0.7) \times 10^{-4}$	$(37.8 \pm 0.1) \times 10^{-4}$
E_0 (keV)	1	1	1
b_2	0	$(1 \pm 0.1) \times 10^{-3}$	
b'_2 (cm^2/keV^2)	$(1.87 \pm 0.02) \times 10^{-10}$	$(0.82 \pm 0.03) \times 10^{-10}$	

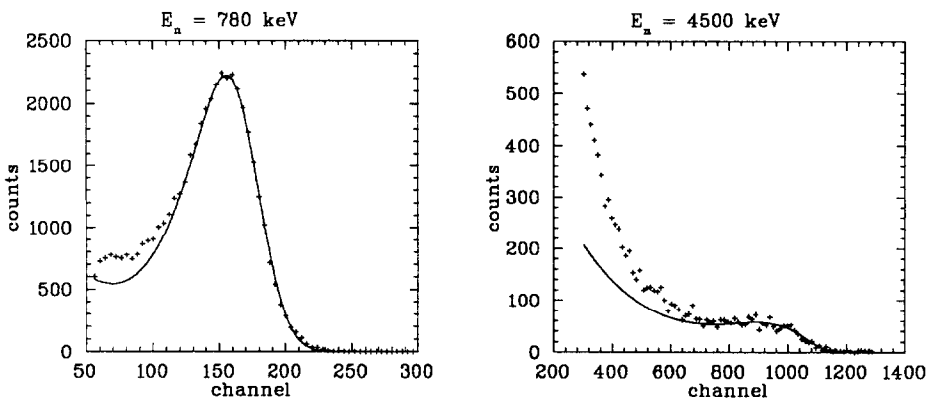

Fig. 6. Comparison of the measured (" + "-symbols) and calculated response functions (full lines) for 780 and 4500 keV.

scintillators due to quenching and is the solution of the differential equation describing recombination. The small value of α around 1 MeV cannot be explained by a ballistic deficit. The primary ionization tracks of 1 MeV alpha particles in ^{4}He are shorter than those of higher-energy alpha particles. This is explained by the fact that the stopping power as a function of the alpha particle energy has a maximum close to 1 MeV. Consequently, these tracks have a small spread of electron drift times. The present data, therefore, suggest an important contribution of recombination effects in the detector at lower energies.

The relative resolution (FWHM) as a function of the E_c^{max} is given in Fig. 5b. The resolution has been tentatively expressed by

$$\sigma^2(E_c) = b_0 + b_2 E_c^2 + b'_2 \left(\frac{dE}{dx} E_c \right)^2 \qquad (18)$$

with parameters b_0, b_2, b'_2. The parameter b_0 has been determined by pulser measurements to be 1 channel^2. At energies above 2 MeV a relative resolution of about 12% is observed for the TGM detector. Since statistical fluctuations are expected to be small, the resolution is mainly determined by the detector design and the electronic processing of the pulses.

The simulated response functions shown in Fig. 6 use the energy and resolution calibrations reported in Fig. 5. It is clear from these graphs that at low energies, measurement and simulation do not agree. This is attributed to scattered neutrons within the experimental hall as will be discussed in more detail below. From these data the total integrated fluence Φ_0 produced by the LiF target can be determined. The results are reported in Fig. 7 and compared to a Monte-Carlo calculation [20]. The neutron background is effectively subtracted with

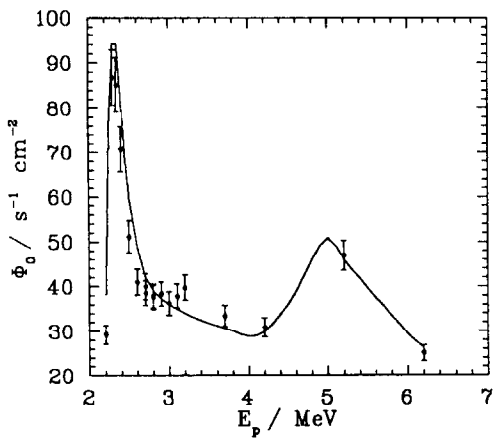

Fig. 7. Total integrated neutron fluence versus energy of the proton beam compared to calculations (full line). The data roughly follow the ^{7}Li(p, n) neutron production cross section as expected.

Table 3
The neutron beams used for the measurements with the RS detector. The 144 keV beam is a filtered reactor spectrum, all other beams were produced at the PTB accelerator facility using the targets indicated. ΔE indicates the energy loss of the charged particles in the target. For the 144 keV reactor spectrum ΔE indicates an estimate of the line width

E_n (keV)	ΔE (keV)	Source
144	14.0	Si-Ti Filter
499	7.8	^{7}Li(pn)
565	7.8	^{7}Li(pn)
795	112.5	^{3}H(pn)
1006	112.5	^{3}H(pn)
1200	112.5	^{3}H(pn)
2500	118.8	^{3}H(pn)
3999	204.4	^{2}H(dn)
5000	204.4	^{2}H(dn)
8035	366.0	^{2}H(dn)
14 860	240.2	^{3}H(dn)

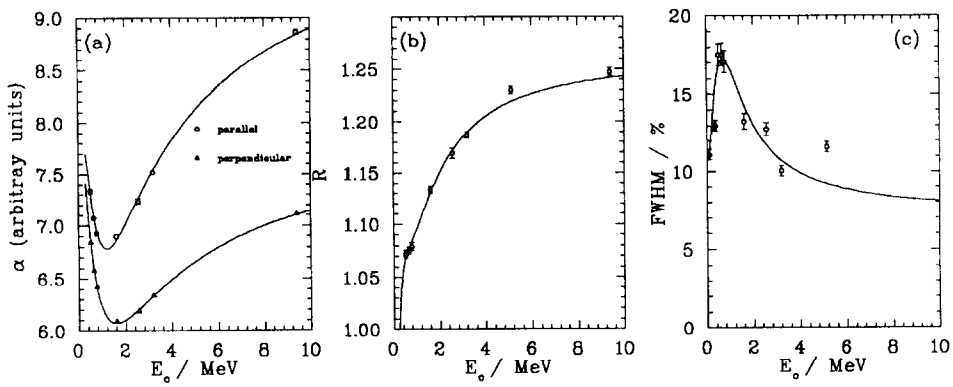

Fig. 8. (a) The function $\alpha(E_e^{max})$ [see Eq. (15)] for the RS detector determined from measurements with the neutron beam parallel and perpendicular to the anode wire. (b) The ratio R of $\alpha(E_e)$ for the parallel and $\alpha(E_e)$ for the perpendicular measurement. (c) The relative resolution (FWHM) for the perpendicular measurements.

the help of the detector simulations since only the events below the full curve in Fig. 6 are counted towards the measured total fluence. Obviously, the agreement between measurement and calculation is quite good indicating that our detector simulation is satisfactory.

For the RS detector, response functions were obtained for neutron energies between 144 keV and 14 MeV at the reactor and accelerator facilities of the Physikalisch-Technische Bundesanstalt (PTB) in Braunschweig. Details of these fields are reported in Refs. [25–27], and are summarized in Table 3. All measurements were performed at a detector position three meters away from the neutron production target. The detector was placed in two different orientations; with the anode wire perpendicular to the neutron beam and with the anode wire parallel to the neutron beam.

The energy and resolution calibration of the RS detector is summarized in Fig. 8 and Table 2. The

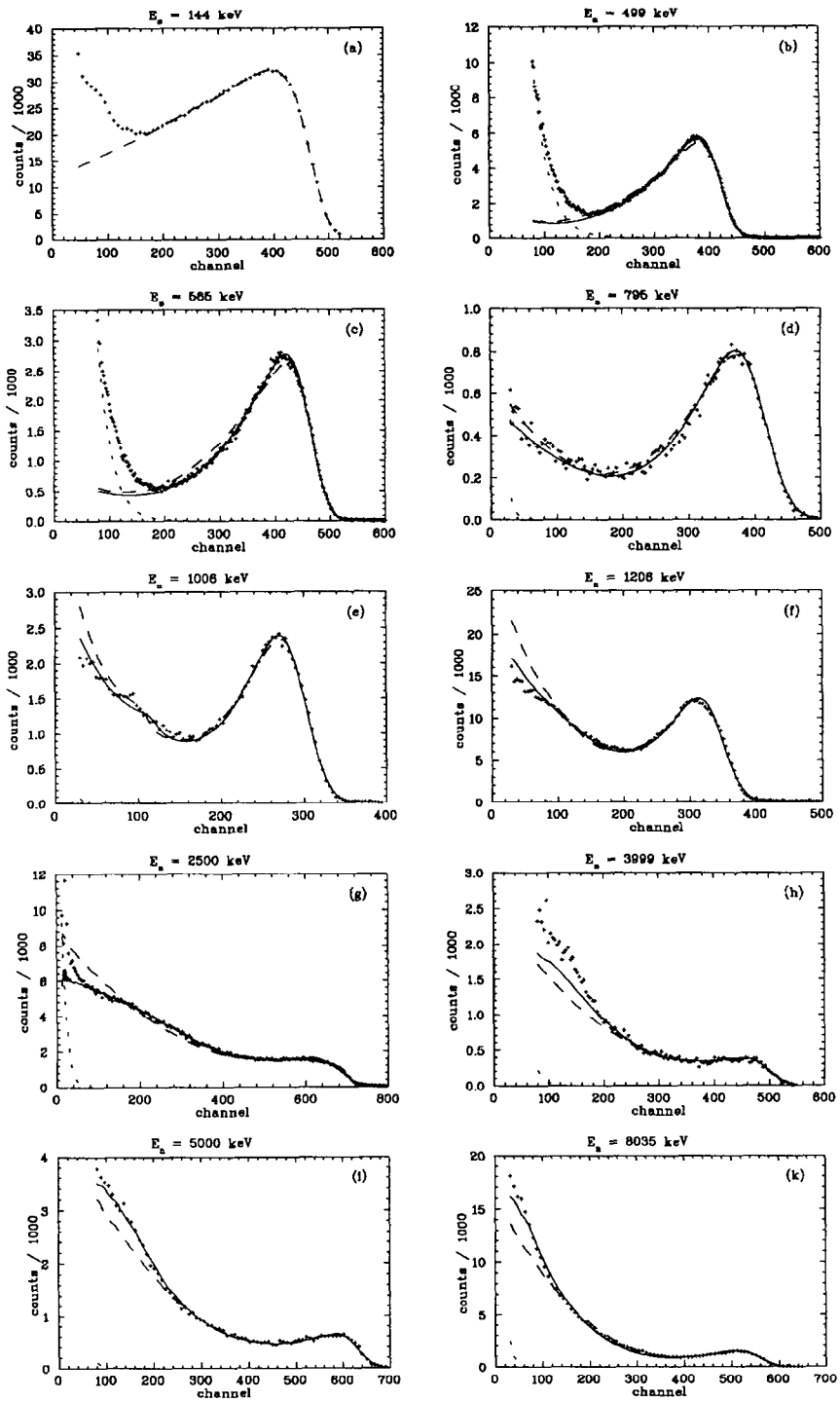

Fig. 9. Comparison of the measured (" + "-symbols) and calculated response functions (full lines) for all measured energies below 10 MeV The long-dashed line is a calculation with a linear energy calibration. The short-dashed line is an exponential fit to the photon background

results are similar to those obtained with the TGM detector. The ratio R between the pulse height measured for the parallel beam and that obtained with the perpendicular beam as a function of recoil energy is given in Fig. 8b. This figure clearly shows that the pulse height measured depends on the direction of the alpha track with respect to the anode wire. This dependence is less at low recoil energies because of the decrease of track length over which primary ionization occurs. This suggests that in calculating the energy deposition within the detector the angular dependence shown in Fig. 8 should be included for each event seperately. Using a shaping time of 12 μs no difference in resolution between parallel and perpendicular geometry is observed for neutron beams below 8 MeV. This suggests a constant ballistic deficit due to the slow drift time of the secondary positive ions. The improved resolution of the RS detector as compared to the TGM detector could be due to both the quality and thickness of the anode wire and the smaller multiplication region. It is important to note that our analysis of measurements with the RS detector assumes monoenergetic neutron beams. A tentative analysis with a neutron energy distribution calculated for selected nominal neutron energies shows that the resolution of this detector is somewhat better than indicated in Fig. 8c.

In the following, a comparison is made between the calculated response functions and the measurement data for all neutron energies investigated with the RS detector at PTB. A summary of the data obtained with neutron energies below 10 MeV is given in Fig. 9. Also shown is a description with a linear energy calibration. It is concluded that the nonlinear energy calibration function (Fig. 8a) is clearly necessary for a good description of the measured response functions. The description for low recoil energies is significantly better than that obtained with the TGM detector. This is due to the fact that room scattering of neutrons is reduced due to the specific design of experimental hall available at PTB. Furthermore, the residual scattered neutron fluence was accounted for by carrying out measurements with a shadow cone in place. The integrated neutron fluence Φ_0 determined from the measurements with the RS detector (Table 4) and the simulation of the detector are in agreement with

Table 4
The total fluence rate Φ [in $(cm^2\ \mu C)^{-1}$] measured with the RS detector in a neutron beam perpendicular to the anode wire, compared to the total fluence rate Φ_0^G obtained from independent measurements with a recoil proton proportional counter or a recoil proton telescope. The quoted uncertainties in parentheses) for Φ_0^G include systematic errors, for Φ_0 they are purely statistical

E_n (keV)	4 μs shaping time		12 μs shaping time	
	Φ_0^G	Φ_0	Φ_0^G	Φ_0
499	9.2 (0.7)	10.00 (0.02)		
565	13.7 (0.9)	13.90 (0.07)		
795	22.2 (1.6)	21.52 (0.09)	20.2 (1.4)	18.73 (0.15)
1006	27.0 (1.9)	26.74 (0.09)	24.5 (1.7)	24.25 (0.15)
1200	41.6 (2.7)	42.01 (0.16)	38.6 (2.5)	36.99 (0.17)
2500			138.3 (8.3)	143.86 (0.58)
3999			7.2 (0.5)	7.74 (0.06)
5000			44.2 (2.7)	44.96 (0.19)
8034			1070.0 (75)	1103.00 (6.00)

the value Φ_0^G determined independently with other detector systems [28]. This also indicates that our description of the RS detector is satisfactory.

As pointed out in the previous section (see Fig. 4), the description obtained for the 14.86 MeV response in perpendicular geometry does not agree well with the data. This was attributed to the electronics which were not capable of handling pulses with very long rise times. This finding is supported by the fact that the same response in parallel geometry is described very well as is shown in Fig. 10. In parallel geometry, most events have short rise times.

In summary, it may be concluded that the response functions of both detectors investigated can well be described up to 10 MeV neutron energy. It appears that the contribution of neutron-induced particle reactions in the counter wall can be neglected. This contrasts with conclusions reached by Birch [12]. The agreement between simulation and the data is very good, this means that it is possible to use commercially available ^{4}He-filled proportional counters in neutron spectrometry applications. Standard unfolding codes can be applied. In the energy range investigated here, NE213 liquid scintillator detectors are usually used for precision neutron spectrometry. In view of the findings

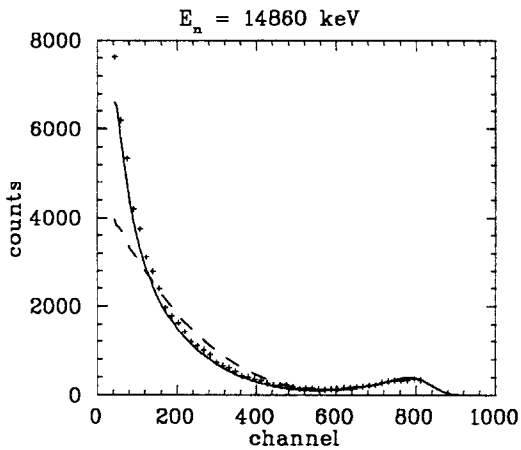

Fig. 10. Comparison of the measured (" + "-symbols) and calculated response functions (full lines) for a 14.86 MeV neutron beam *parallel* to the neutron beam. The long-dashed line is a calculation with linear energy calibration.

presented in this paper, ^{4}He-filled detectors may be a suitable alternative.

Acknowledgements

The authors would like to thank the operating staff of the accelerator and reactor of PTB, Braunschweig, and the accelerators at INFN, Legnaro, and the University of Tübingen for providing the neutron beams and technical support. In particular, we thank Dr. E. Dietz, Dr. U. Graf, Dr. S. Guldbakke, W. Sosaat, and W. Wittstock for technical advice. Dr. Guldbakke provided the results of the total fluence measurements with the proton recoil telescope and other detectors reported for comparison in Table 4. We thank Dr. H. Klein, Dr. K. Knauf and Dr. B. Siebert for carefully reading the manuscript. Special thanks are due to Dr. K. Knauf and M. Looman for their interest in the present work and the many discussions and suggestions.

References

[1] R. Batchelor, R. Aves, T.H.R. Skyrme, Rev. Sci. Instr. 26 (1955) 1037.
[2] E.F. Benett, Rev. Sci. Instr. 26 (1962) 1153.
[3] P.W. Benjamin, C.D. Kemshall, J. Redfearn, Nucl. Instr. and Meth. 59 (1968) 77.
[4] R. Birch, M. Marshall, L.H.J. Peaple, AERE Report R-11398, 1984.
[5] E. Dietz, M. Matzke, W. Soosat, G. Urbach, M. Weyrauch, Nucl. Instr. and Meth. A 332 (1993) 521.
[6] N.L. Snidow, H.D. Warren, Nucl. Instr. and Meth. 51 (1967) 109.
[7] R. Gold, E.F. Bennet, Nucl. Instr. and Meth. 63 (1968) 285.
[8] K. Weise, M. Weyrauch, K. Knauf, Nucl. Instr. and Meth. A 309 (1991) 287.
[9] E. Baldinger, P. Huber, H. Straub, Helv. Phys. Acta 11 (1938) 245.
[10] H.F. Atwater, Nucl. Instr. and Meth. 100 (1972) 453.
[11] P.J. McDaniel, H.E. Hungerford, Nucl. Instr. and Meth. 165 (1979) 509.
[12] R. Birch, AERE Report R-13002, 1988.
[13] R.E. Shamu, Nucl. Instr. and Meth. 14 (1961) 297.
[14] P.F. Rose, C.L. Dunford (Eds.), ENDF-102, Data formats and procedures for the evaluated nuclear data file ENDF, Brookhaven National Laboratory, Upton, New York, March 1990.
[15] M. Weyrauch, A. Casnati, P. Schillebeeckx, GNSR A computer code to calculate response functions of gas-filled neutron detectors, Physikalisch-Technische Bundesanstalt, Report PTB-N-26, Braunschweig, 1996, ISBN 3-89429-730-1.
[16] A. Casnati, M. Weyrauch, P.Schillebeexkx, in: G. Vourvopoulos (Ed.), International Conf.: Neutrons in Research and Industry, Proc. SPIE, vol. 2867, 1997, p. 445.
[17] P. Schillebeeckx, A.Casnati, M. Clapham, U. Graf, M.Looman, M. Weyrauch, in: G. Vourvopoulos (Ed.), International Conf.: Neutrons in Research and Industry, Proc. SPIE, vol. 2867, 1997, p. 631.
[18] M. Matzke, Unfolding of pulse height spectra: the HEPRO program system, Physikalisch Technische Bundesanstalt Report PTB-N-19, Braunschweig, 1994, ISBN 3-89429-543-0.
[19] K. Knauf, J. Wittstock, Neutron spectrometry with proton recoil proportional counters at the research and measuring reactor Braunschweig, Report PTB-FMRB-114, Braunschweig, 1987.
[20] M. Looman, private communication.
[21] J.F. Ziegler, The Stopping Power and Ranges of Ions in Matter, Pergamon Press, New York, 1985.
[22] E.C. Finch, Nucl. Instr. and Meth. 113 (1973) 41.
[23] G.B. Birks, Phys. Rev. 84 (1951) 364.
[24] G.B. Birks, Proc. Phys. Soc. A 64 (1951) 874.
[25] W.G. Alberts, E. Dietz, Laboratory Report, PTB-FMRB-112, (1987).
[26] M. Matzke, K. Knauf, E. Dietz, A. Plewnia, W.G. Alberts, 7th ASTM-Euratom Symposium on Reactor Dosimetry, Strasbourg, France, 27–31 August 1990.
[27] S. Guldbakke, S. Dietz, H. Kluge, D. Schlegel, in: W. Kölzer, H. Maushart (Eds.), Strahlenschutz: Physik und Messtechnik, vol. 1, Verlag TÜV Rheinland, Köln, 1994, p. 240.
[28] S. Guldbakke, private communication.